University of Tennessee, Knoxville
Trace: Tennessee Research and Creative Exchange

Faculty Publications and Other Works -- Materials Science & Engineering

Engineering -- Faculty Publications and Other Works

4-2014

Nanomaterials synthesis by a novel phenomenon: The nanoscale Rayleigh-Taylor instability

S. Yadavali
University of Tennessee - Knoxville, syadaval@vols.utk.edu

Ramki Kalyanaraman
University of Tennessee - Knoxville, ramki@utk.edu

Follow this and additional works at: http://trace.tennessee.edu/utk_matepubs

Part of the Materials Science and Engineering Commons

Recommended Citation

Yadavali, S., and R. Kalyanaraman. "Nanomaterials Synthesis by a Novel Phenomenon: The Nanoscale Rayleigh-Taylor Instability." AIP Advances 4, no. 4 (2014). DOI: 10.1063/1.4871482.

Nanomaterials synthesis by a novel phenomenon: The nanoscale Rayleigh-Taylor instability

S. Yadavali and R. Kalyanaraman

Articles you may be interested in

Nanoparticle generation and transport resulting from femtosecond laser ablation of ultrathin metal films: Time-resolved measurements and molecular dynamics simulations
Appl. Phys. Lett. **104**, 193106 (2014); 10.1063/1.4876601

Alignment of gold nanorods by angular photothermal depletion
Appl. Phys. Lett. **104**, 083118 (2014); 10.1063/1.4867016

Femtosecond laser welded nanostructures and plasmonic devices
J. Laser Appl. **24**, 042001 (2012); 10.2351/1.3695174

Sharpening the shape distribution of gold nanoparticles by laser irradiation
J. Appl. Phys. **100**, 084311 (2006); 10.1063/1.2358822

Space and time resolved temperature measurements in laser pulse-produced metal melts
Rev. Sci. Instrum. **68**, 2534 (1997); 10.1063/1.1148155

Nanomaterials synthesis by a novel phenomenon: The nanoscale Rayleigh-Taylor instability

S. Yadavali[1] and R. Kalyanaraman[1,2]
[1]*Department of Chemical and Biomolecular Engineering, University of Tennessee, Knoxville, TN 379996*
[2]*Department of Material Science and Engineering, University of Tennessee, Knoxville, TN 37996*

The Rayleigh-Taylor (RT) interfacial instability has been attributed to physical phenomenon in a wide variety of macroscopic systems, including black holes, laser generated plasmas, and thick fluids. However, evidence for its existence in the nanoscale is lacking. Here we first show theoretically that this instability can occur in films with thickness negligible compared to the capillary length when they are heated rapidly inside a bulk fluid. Pressure gradients developed in the evaporated fluid region produce large forces causing the instability. Experiments were performed by melting Au films inside glycerol fluid by nanosecond laser pulses. The ensuing nanoparticles had highly monomodal size distributions. Importantly, the spacing of the nanoparticles was independent of the film thickness and could be tuned by the magnitude of the pressure gradients. Therefore, this instability can overcome some of the limitations of conventional thin self-organization techniques that rely on film thickness to control length scales. © *2014 Author(s). All article content, except where otherwise noted, is licensed under a Creative Commons Attribution 3.0 Unported License.* [http://dx.doi.org/10.1063/1.4871482]

I. INTRODUCTION

There are many applications of nanostructures, such as nanoparticles (NPs), of any variety of hard matter, including metals, ceramics and semiconductors, that require their arrangement on surfaces with precise control over size and spacing. Some broad categories of applications include solar energy harvesting, biosensing, and photocatalysis.[1–9] In recent years the spontaneous deformation of a thin film leading to nanoscale patterns governed by self-organizing principles have generated great interest. The reason is that by controlling the choice of materials, such as film and substrate, intrinsic forces of surface tension and dispersion can be changed to modify the time and length scales of pattern formation.[10–12] However, while the reliance of intrinsic forces leads to robustness and predictability in pattern formation, such thin film self-organization invariable limits the control over pattern length scale to the form $\lambda \propto h^n$, where λ is the self-organized length, h is the film thickness and n varies depending on the conditions used. For instance, in the well studied *liquid-phase* spinodal dewetting instability, the pattern length scale λ varies with film thickness h as $\lambda \propto h^2$[11,13–15] and could be modified somewhat by introducing thermal gradients,[16] or by relying on solid state mass transport.[17] While some other ways to overcome this constraint have been demonstrated for polymer liquid films, such as by chemical or morphological modifications to the substrate surface,[18–20] similar flexibility has not been shown for the vast majority of high temperature fluids, such as metals and semiconductors.

Here we propose a novel way to decouple the self-organized length scale from film thickness by using the Rayleigh-Taylor (RT) instability. From a historical perspective, the length scale in the *classical* RT pattern-forming instability, such as the beading up of a water film on the ceiling, does not depend on the thickness of the film.[21] But, the *classical* RT instability cannot be observed in nanoscale thin films because the acceleration forces acting on the fluid come from gravity, thus

requiring thick films (thickness greater then the capillary length of order 0.1 mm). On a fundamental level, the primary requirement for the RT instability is that a less dense fluid should be accelerated into a more dense fluid.[22,23] This interface destabilization between two fluids can be achieved in a number of different ways,[21] as evident by the large number of examples from an extremely diverse range of systems, including in astronomical structures such as black holes and supernova,[24–26] geophysical phenomenon,[27,28] fusion,[29–32] and bulk fluid-fluid interfaces.[33–35]

The new idea proposed in this work is based on the interesting thermal behavior found when a film-fluid interface is heated rapidly by short laser pulses, with the fluid being converted into gas. Since the temperature falls rapidly on going away from the film/gas interface, strong gas pressure gradients are generated. This leads to a local, film-thickness-dependent, pressure that can overcome the stabilizing effects of surface tension and also dominate the destabilizing effects of intermolecular attractions found in nanoscale thickness films. When this result is incorporated into mass transport models, linear analysis predicts a classical RT instability scaling behavior. We performed experiments involving nanosecond (ns) pulsed laser melting of nanometer thick Au films immersed in glycerol liquid. The ensuing nanoparticle size and spacing was studied as a function of laser energy and film thickness. The results were in excellent agreement with the theoretical predictions of the RT instability, including the independence of nanoparticle spacing on film thickness. To the best of our knowledge this is the first observation of RT instability at the nanoscale and its application towards synthesizing materials in a controllable manner.

II. BACKGROUND

In the macroscopic or classical RT instability, a liquid film hanging on a substrate is destabilized when gravitational effects overcome the pressure exerted by the ambient atmosphere.[21] In this work we are primarily concerned with films whose thickness is substantially smaller then capillary lengths, which, for example, is of the order of 0.1 mm for the metal films we will investigate here. In this situation, gravity cannot play a role in stabilizing/destabilizing the film. Instead, other mechanisms to destabilize the films exist. One widely studied case pertains to the scenario when intermolecular attractive forces, such as dispersion forces, can overcome surface tension and result in spontaneous dewetting. This phenomenon has been widely investigated in organic and inorganic films in the context of spinodal dewetting and is typically exhibited by ultrathin films (normally <100 nm).[12,36–38] The characteristic feature of this instability is the strong dependence of the pattern length scale on the film thickness, i.e. $\lambda_{dewet} \propto h_o^2$, where h_o is the initial film thickness.[14,15]

First, we describe a general scenario in which an RT-like instability can arise in nanometer thick films lying *on* a substrate, as shown in Fig. 1(a). Picture a surface perturbation of the liquid film shown in Fig. 1(a) occurring into a hydrostatic pressure field where the pressure acting on the film is dependent on the local height of the film at any position x along the perturbed film, i.e. $p(h) = P(x, z)$. Two possible situations can be envisioned. In the first case, let the local pressure increase with increasing film height h. In this situation, the increased pressure will counter the growth of the perturbation (adding to the effect of surface tension) and therefore, increase the overall stability of the film to deformations. On the other hand, consider the case when the local $p(h)$ *decreases* with increasing h. In this case, the pressure field opposes the stabilizing effect of surface tension and, if it is large enough, can foster the growth of the perturbation, leading eventually to spatial and temporal behavior dependent on the various forces in play. Recently, two physical processes to achieve this type of scenario have been postulated. Bestehorn *et al.*[39] suggested the theoretical possibility that a thin film on the underside of a substrate (i.e. RT unstable film) in equilibrium with its vapor phase under a steady-state thermal gradient can lead to patterns influenced by the evaporative process. A second possibility, a non-gravitationally generated RT instability, was reported as an experimental observation by Chen *et al.*[40] in which the pulsed laser melting of a *bulk* Si surface immersed in water produced patterns that resemble the early-stage hexagonal structures predicted by the Cahn-Hillard form of the RT evolution. The physical mechanism invoked was the explosive boiling of water in contact with the Si surface, which could generate sufficient pressures to produce the resulting patterns. However, the physical origin of the local $p(h)$ behavior described above that is essential to destabilize the surface was not discussed. In addition, an important quantitative hallmark of the
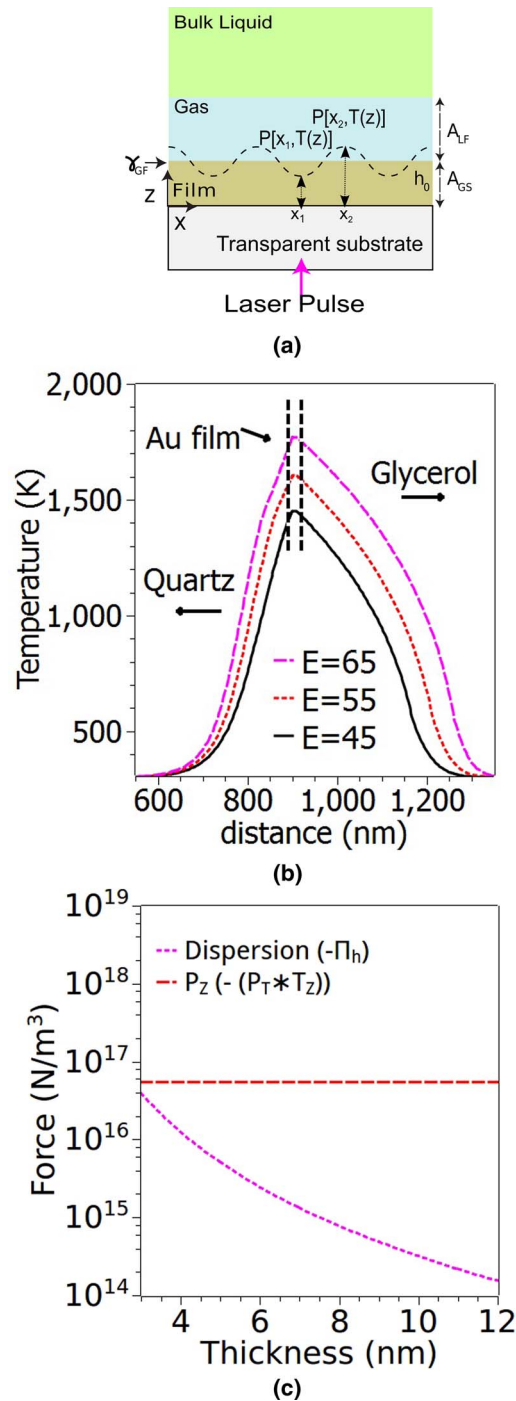
(a)

(b)

(c)

FIG. 1. (a) Schematic illustration of the mechanism of RT instability based on thermally-induced pressure gradients. Laser heating of the substrate/film/fluid system vaporizes the fluid and produces large thermal gradients perpendicular to the ensuing film/vapor interface. Fluctuations about the average film height h_o are amplified when the gas pressure is a function of height z and $P[x_1, T(z)] > P[x_2, T(z)]$. Also depicted are various other forces on the film, such as intermolecular dispersion forces with magnitude determined by the Hamaker coefficients A_{ij} of the various pairs of interfaces and the surface tension forces. (b) Thermal model calculations of nanosecond (ns) pulsed laser heating of the quartz/Au(8 nm)/glycerol system for various laser energy densities (in mJ/cm^2) predict large thermal gradients $T_Z = dT/dz$, of the order of 30K/nm can exist in the gas. The position of the Au film is indicated by the dashed vertical lines. (c) Estimated values of the pressure gradient P_Z forces (dashed line) based on the known P vs T behavior of glycerol when the film peak temperature was set to be T*=1750 K. These magnitudes, of the order of $\sim5\times10^{16}$ Pa/m, are substantially larger then the dispersion forces acting in this system (dotted line).

RT instability, which is its characteristic length scale λ was not presented. The length scale of RT instability patterns should behave as $\lambda \propto \sqrt{\frac{2\gamma}{\rho a}}$, where γ is the surface tension of the film (or bulk) surface and ρa characterizes the effective pressure per unit length (force per unit volume) arising under the acceleration a.[21] It should be emphasized that such non-gravitationally induced RT instability behavior has not been experimentally verified in reported works for either bulk or thin fluid films, including in situations producing patterns with characteristic length scales in the nanometers.

We propose an alternate way to foster RT instabilities based on the thermal profile that occurs at a substrate/film/fluid interface that is rapidly heated by a short laser pulse. The rapid heating of the film by absorption of short [*such as nanosecond (ns)*] pulse laser light is well known to lead to boiling of a low temperature fluid in contact with the film.[41–43] Because of the rapid heating rates, a large drop in temperature occurs on going away from the absorbing film, i.e. a large magnitude of thermal gradient $|T_Z| = |\frac{dT}{dZ}|$ with a negative sign (i.e. $T_Z < 0$, indicating decrease in temperature in going from the interface into the vapor/fluid region) exists. When these thermal gradients are incorporated into the pressure dependence of temperature of the gas phase, large transient gas pressures, that *fall* with distance away from the film, develop. This pressure gradient $P_Z = \frac{dP}{dZ}$, with sign $P_Z < 0$, can produce a local film thickness-dependent gas pressure $P[x, T(z)]$ [Fig. 1(a)] such that it drives the fluid to flow from regions of locally lower film thickness to higher ones, i.e. grows perturbations and produces the RT instability, as we demonstrate in the remainder of this manuscript.

III. THEORY AND MODELING

The estimate of pressure gradients P_Z perpendicular to a film/gas boundary was evaluated with specific reference to the ns pulsed laser heating of a quartz/Au/Glycerol system irradiated by 266 nm wavelength laser light at normal incidence from the quartz side. At this wavelength, the photons are absorbed only by the Au film layer (and are transparent to quartz and Glycerol).[44] The ensuing physical situation for laser energies of relevance here resulted in the melting of the Au film, as well as the formation of a gas phase region of Glycerol bounded by its fluid on one side and the molten Au film on the other, as shown in the schematic, Fig. 1(a). First, a simple order of magnitude estimate (and sign) of the pressure gradient P_Z in the vapor was made by estimating a temperature gradient T_Z away from the film/gas interface through a thermal diffusion analysis as follows. For the T_Z in glycerol, we assumed that the spatial extent of the vaporized glycerol L_{gl}^v can be approximated as one thermal diffusion length, i.e. $L_{gl} = \sqrt{D_{gl}^{Th}\tau_p}$, where D_{gl}^{Th} and τ_p are the thermal diffusivity of liquid glycerol and the laser pulse time respectively. Using D_{gl}^{Th} of 10^{-9} m^2.s^{-1} from Ref. 45, and using a laser pulse width of 9 ns, we get L_{gl} of $\sim$30 nm. The simplest approximation for the gradient is a linear one between the melting point of Au (1337.3 K) on the film side to boiling point of glycerol (563 K) on the glycerol vapor/fluid boundary side. This gives an order of magnitude for the thermal gradient, T_Z, as ~ -25 K/nm, with the negative sign indicating that the temperature decreases in going from the interface into the Glycerol vapor/fluid region. Now, the $P_T = dP/dT$ for glycerol from P vs T empirical data available from standard references[45] varies with T and is $\sim 5 \times 10^6$ Pa/K at the melting point of Au. In other words the transient pressure gradient P_Z is estimated to be $\sim -1.25 \times 10^{17}$ Pa/m, and is a negative quantity, consistent with the sign of T_Z and the positive sign of P_T typically seen in gases. Therefore, for a metal like Au with density of $\sim 20 \times 10^{-3}$ Kg.m^{-3}, by using the dimensional equality of $|P_Z| = |\rho a| = |P_T \times T_Z|$, we get an extremely high value for the acceleration a of $\sim 6 \times 10^{19}$ m^2/s, substantially larger then the estimates of Chen *et al.*[40] To better quantify this thermal effect, we performed finite element calculations to estimate the T_Z (and thereby P_Z) based on Fourier heat transport models for multilayer heating that incorporate phase change effects. We have previously developed these models in Refs. 12 and 46, where appropriate use of thermally varying materials parameters allowed us to successfully explain the thermal transport behavior in such nanoscale systems. The Fourier heat transport form of thermal transport was expressed as follows:

$$\rho C_p \frac{\partial T}{\partial t} = \nabla[k\nabla T] + Q_{laser}(z, t) \tag{1}$$

This equation was solved in each material layer, with ρ being the mass density of the layer, C_p the isobaric heat capacity, k the thermal conductivity, z the axis normal to the planar, fixed surface pointing from the substrate, as shown in Fig. 1(a), and $Q_{laser}(z, t)$ being the laser heating contribution given by $Q_{laser}(z, t) = A(z)(1 - R(z))I(t)exp[-A(z)z]$, where $R(z)$ is the thickness dependent reflectivity, and $A(z)$ is the thickness dependent absorption coefficient. $R(z)$ and $A(z)$ were calculated using the rigorous method described in Ref. 47. The temperature dependent ρ, C_p and k for glycerol liquid and gas phase were calculated from Ref. 48 and for gold from.[49] The incident laser power was modeled as a Gaussian distribution with 9 ns pulse width, consistent with the characteristics of the laser used in the experiments to be described. Further details of the calculation are provided in the supplemental information Sec. II and in supplement Fig. 1.[50]

In Fig. 1(b), temperature vs distance behavior at the time corresponding to the peak temperature rise in a 8 nm thick Au film for various laser energy densities is shown. The large change in temperature with distance away from the film/gas interface (as well as film/substrate interface) is clearly evident and was calculated to be of the order of magnitude of 30 K/nm at the time of the peak temperature T^*. The gradients were estimated from these T vs distance plots as follows. A linear interpolation was applied between the position of the peak temperature at the film/gas interface to the position in the gas phase when the temperature dropped to the glycerol phase change temperature (T = 563 K). Next, by using the empirically known P vs T for glycerol,[45] the effective pressure force, P_Z, was estimated for films of various thickness by selecting the laser energy density to achieve the same maximum temperature rise (of $T^* = 1750$ K). The magnitude of the obtained P_Z is shown by the dashed line in Fig. 1(c). The two important features are its large magnitude, i.e. $O(10^{16})$ N/m^3, and its relative independence to the thickness of the film (for the same peak temperature T^*). As we discuss shortly, the magnitude of this P_Z force (in Pa/m or N/m^3) is substantially larger then other destabilizing forces, such as the intermolecular dispersion forces estimated for the quartz/Au system[49] and shown by the dotted line in Fig. 1(c).

To theoretically evaluate the role of this large P vs z on film behavior, we solved the mass transport dynamics using the thin-film hydrodynamic equation in the lubrication approximation of the Navier-Stokes equations.[51] This form allowed us to include the gas pressure in addition to the surface tension and dispersion forces due to intermolecular interactions that are already present in such ultrathin film on substrate systems, as depicted in Fig. 1(a).[13,52] A similar approach to solving for the hydrodynamics has been used by us previously in Ref. 12 and 46 to explain the linear and non-linear dynamics of ultrathin fluid films. The total pressure $P(x, z)$ acting on the film at position x was expressed as the superposition of a disjoining pressure (Π), Laplace pressure P_L and pressure due to the gas layer $P[T(z(x))]$, as:

$$P(x, z) = P_L + \{\Pi(z) - \Pi(h(x))\} - P[T(z(x)]\tag{2}$$

We solved for the evolution of the instantaneous film height h in 1-dimensions (1D) by the mass conservation equation of the form

$$\frac{\partial h(x)}{\partial t} = -\frac{h^3}{3\mu}\frac{\partial}{\partial x}\frac{\partial}{\partial x}\{\gamma\frac{\partial^2 h(x)}{\partial x^2} + \frac{d\Pi}{dh}.h(x) + P[T(z(x)]\}\tag{3}$$

Where γ is the surface tension of the film-gas interface [γ_{GF} in Fig. 1(a)], η is the viscosity of the film, and the disjoining pressure Π for a thin film on substrate is given by ($\frac{A}{6\pi h_o^3}$), where A is the Hamaker coefficient. Since the gas pressure acting at any point along the film surface is dependent on the temperature through its dependence on height, i.e. $P(x, z) = P[T(z(x)]$, it's spatial derivative can be expressed as follows.

$$\frac{\partial P(x)}{\partial x} = \frac{dP}{dT}\frac{dT}{dz}\frac{\partial z(x)}{\partial x} = P_Z\frac{\partial z(x)}{\partial x}$$

Now since z is the coordinate measuring the height h(x), we can express the 1st and 2nd order spatial derivatives of pressure as $P_Z\frac{\partial h(x)}{\partial x}$ and $P_Z\frac{\partial^2 h(x)}{\partial x^2}$, respectively, yielding an evolution equation of the form:

$$\frac{\partial h(x)}{\partial t} = -\frac{h^3}{3\mu}\frac{\partial}{\partial x}\frac{\partial}{\partial x}\{\gamma\frac{\partial^2 h(x)}{\partial x^2} + \frac{d\Pi}{dh}.h(x)\} - \frac{h^3}{3\mu}P_Z\frac{\partial^2 h(x)}{\partial x^2}\tag{4}$$

Here, we have ignored any contribution to film evolution resulting from the evaporation of the film material during the heating process. As shown in the supplement Fig. 2,[50] actual estimates of Au evaporation based on time and temperatures achieved here suggested negligible contributions. We also chose to ignore the dispersion force contributions, A_{VF} in Fig. 1(a), acting across the glycerol fluid/glycerol gas and glycerol gas/metal film interfaces. This can be justified due to the large thickness of the gas layer (~150 nm based on thermal model estimates) and partly due to the small values of A that typically exist across a gas medium. Therefore, the primary contribution came from the A_{VS} term in the dispersion forces. Equation (4) was solved using linear stability analysis under boundary conditions of no slip at the film/substrate surface $v_z = 0$ at $z = 0$, and no shear stress ($\frac{\partial v_z(z=h)}{\partial x} = 0$) at the film/gas interface with sinusoidal perturbations of form $h(x) = h_o + \varepsilon sin(kx)cos(\omega t)$. This yielded a dispersion relation for deformation rate ω to wavevector k as:

$$\omega = \frac{h^3}{3\eta} \left[-\gamma k^4 - \Pi_h k^2 - P_Z k^2 \right] \tag{5}$$

Where $\Pi_h = -\frac{A}{2\pi h^4}$, with the negative value signifying an attractive term (with the Hamaker coefficient taken as a positive quantitiy), and the pressure gradient P_Z also having a negative sign, as explained earlier. From this, the characteristic wavelength $\lambda_{RT} = 2\pi/k_m$ was obtained from the maximum growth rate of perturbations k_m (i.e. $k_m^2 = \frac{-\Pi_h - P_Z}{2\gamma}$, when $\frac{d\omega}{dk} = 0$) as:

$$\lambda_{RT}^2 = \frac{8\pi^2 \gamma}{\frac{A}{2\pi h_0^4} - P_Z} \tag{6}$$

Also, the time scale $\tau_{RT} = \frac{2\pi}{\omega_m}$ associated with the growth of perturbations with wavelength λ was obtained by letting $k = k_m$ in Eq. (5), giving:

$$\tau_{RT} = \frac{6\pi\eta}{h_o^3(-\gamma k_m^4 - \Pi_h k_m^2 - P_Z k_m^2)} \tag{7}$$

IV. EXPERIMENTS

To analyze the implications of this model, experiments were performed for Au films (with thickness ranging from 4 to 12 nm) deposited on transparent bulk quartz (SiO_2) substrates, with this system immersed in a bulk glycerol liquid solution. The Au films were deposited in high vacuum ($\sim 1 \times 10^{-8}$ Torr) by electron beam deposition at room temperature onto commercially obtained, optical quality, SiO_2 substrates.[15] The deposition rate used here was typically $\backsim$1.5 nm/min as confirmed by atomic force microscope (AFM) step height measurements. Energy dispersive X-ray spectrometry (EDS) was used to measure the Au counts of the deposited films in a scanning electron microscope (SEM). The EDS counts were converted into an equivalent thickness value by using calibration based on step-height measurements of the film thickness. Surface roughness of the deposited films were measured by AFM and established an upper limit of 0.5 ± 0.2 nm for the average root mean square (RMS) roughness over the entire thickness range. The Au/SiO_2 samples were placed on the bottom a transparent glass beaker (with substrate side of the sample in contact with the beaker) filled with pure glycerol. Laser irradiation was performed at normal incidence from the quartz side, as depicted in Fig. 1(a), with an unfocused laser beam of area 1×1 mm^2 at a repetition rate of 50 Hz for a total of approximately 5000 pulses ($\sim$100 seconds). Following the irradiation, the samples were removed from the fluid, dried in air, and the resulting nanostructures were investigated in a scanning electron microscope (SEM) for various values of initial film thickness h_o, and the laser energy density E.
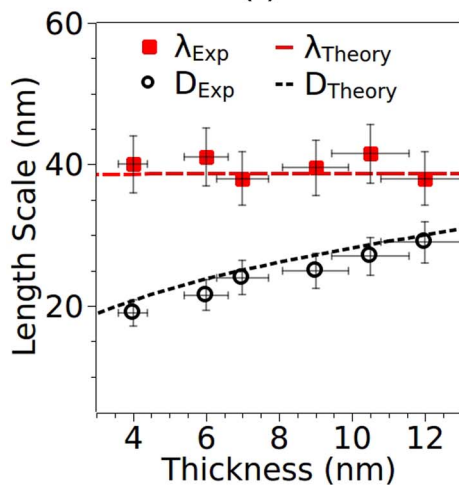
V. RESULTS AND DISCUSSION

Fig. 2(a) shows an SEM image of the prototypical nanostructure obtained following the laser irradiation experiment, in this case for a 4 nm Au film (at 80 mJ/cm^2 energy density). Nanoparticles with a well-defined inter-particle spacing and highly monomodal size distribution were obtained.
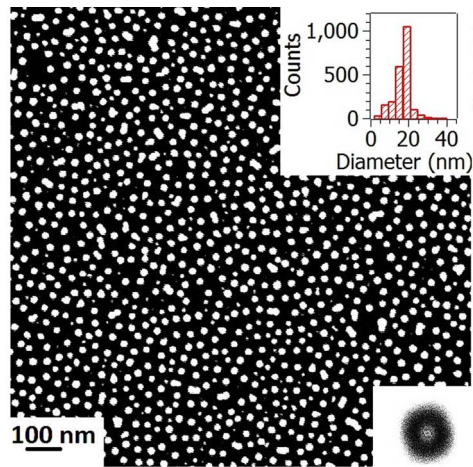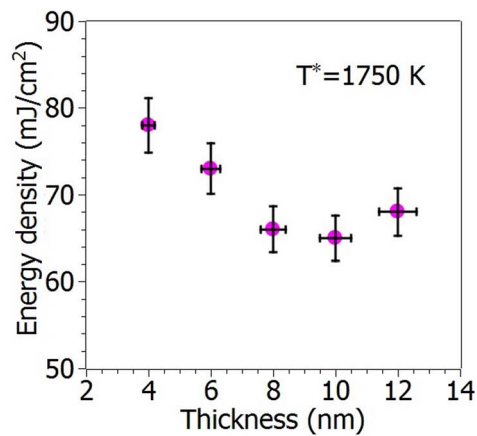
FIG. 2. (a) SEM image of Au nanoparticles formed on quartz following pulsed laser melting of 4 nm Au film in glycerol fluid at laser energy density E = 80 $\frac{mJ}{cm^2}$. Top inset shows the monomodal size via the size histogram of the nanoparticles with diameter $D = 17 \pm 3$ nm. Bottom inset shows an annular FFT behavior of the contrast in the SEM image, indicating short range spatial order in the nanoparticle arrangement. (b) Thermal modeling predictions of the laser energy required to maintain the same peak temperature $T^* = 1750$ K in quartz/Au/glycerol systems with different Au film thickness. (c) Experimental measurements (symbols) vs theoretical predictions (lines) for the spacing (closed symbol) and diameter (open symbol) of nanoparticles as a function of film thickness.

The lower inset in the figure shows the fast fourier transform (FFT) of the contrast in the SEM images. The annular form of the FFT captures the spatial short range ordering typically prevalent in such thin film instabilities. The FFT analysis also allowed accurate calculations of the characteristic nanoparticle spacing. The particle size histogram (upper inset), showed that the standard deviation from the average size was less then 20%, consistent with the definition of a monomodal distribution used in chemical synthesis routes.[53] Such histograms allowed accurate determination of particle diameter.

One of the key implications of the theory (Eq. (6)) is that when the magnitude of the thermal forces given by P_Z are substantially larger then the dispersion forces ($A/2\pi h^4$) then the RT instability length scale should have no explicit dependence upon the film thickness. Indeed, as found by our thermal modeling calculations earlier, and depicted in Fig. 1(c), our experimental situation should be dominated by the P_Z forces, and hence the observed length scale should be explicitly independent of the film thickness and be given by:

$$\lambda_{RT} = 2\pi \sqrt{\frac{2\gamma}{-P_Z}} \tag{8}$$

To test this result, we performed experiments as a function of various Au film thickness by maintaining a similar magnitude of the P_Z forces. This was achieved by first obtaining a laser energy density that resulted in identical maximum temperature of $T^* = 1750$ K for the different thickness via thermal model calculations. This temperature was chosen for ease of experimental purposes. The modeling result to determine the laser energy density is shown in Fig. 2(b) (*this result was, in turn, used previously in Fig. 1(b) to generate the P_Z force values*). In Fig. 2(c) the experiment (closed symbols) and theory predictions (dashed line) for the nanoparticle spacing versus film thickness are shown for similar P_Z. Excellent agreement in trend and magnitude between theory prediction and experimental measurement is evident, strongly implying that the RT instability was responsible for the observed nanoparticles. In addition, the length scale was virtually independent of the film thickness, supporting the hypothesis of a classical RT-like instability.

In Fig. 2(c), the experiment (open symbols) and theory prediction (dotted line) for the nanoparticle diameter versus film thickness is also shown. If the initial volume of material is conserved during the laser irradiation process, the final diameter can be predicted from the characteristic length scales to be $D = c(\theta)(\lambda_{RT}^2 h_o)^{1/3}$,[12] where the constant $c(\theta)$ will be a function of the contact angle of the droplets. Since our thermal model calculations and the known temperature-dependent evaporation rate of Au predicted extremely small material loss due to evaporation effects (result provided in the supplement Fig. 2[50]), we applied volume conservation analysis to the measured nanoparticle size and spacing. Using a hemispherical particle size, which gives a diameter of $D = (\frac{3}{2}\lambda^2 h_o)^{1/3}$, very good agreement in experiment and theory was found.

One of the well-known features of the classical RT instability is the appearance of hexagonal patterns during the early stages of deformation. In our experimental results, we are unable to capture these early stage features due to the extreme rapidity of the process. We estimated the time scales from Eq. (7) and found them to be of the order of $\sim O(10^{-10} - 10^{-11})$ sec for the various laser energy and film thickness conditions explored here, as shown in Fig. 3(a). Since this time scale is substantially smaller then the laser pulse width of 9 ns, therefore, it was only possibly to observe the final ripened structures following destabilization of the film by the gas pressure driven RT instability process. From Fig. 3(a), it can also be noted that the RT instability time scale is much smaller then the spinodal dewetting time scale for all conditions investigated here, consistent with the much larger forces driving the RT instability effect. One of the interesting behaviors of the RT instability is the linear stability analysis prediction of a decrease in time scale with increasing film thickness. By assuming a negligible dispersion force, the RT instability time scale can be expressed as $\tau_{RT} = \frac{24\gamma\pi\eta}{h_o^3 P_Z^2}$, which is in stark contrast to spinodal dewetting in which the time scale varies as $\tau \propto h_o^5$.

Equation (8) suggested that the RT instability length scale will be independent of the film thickness, and its confirmation was presented in Fig. 2(c). That figure also showed that the particle
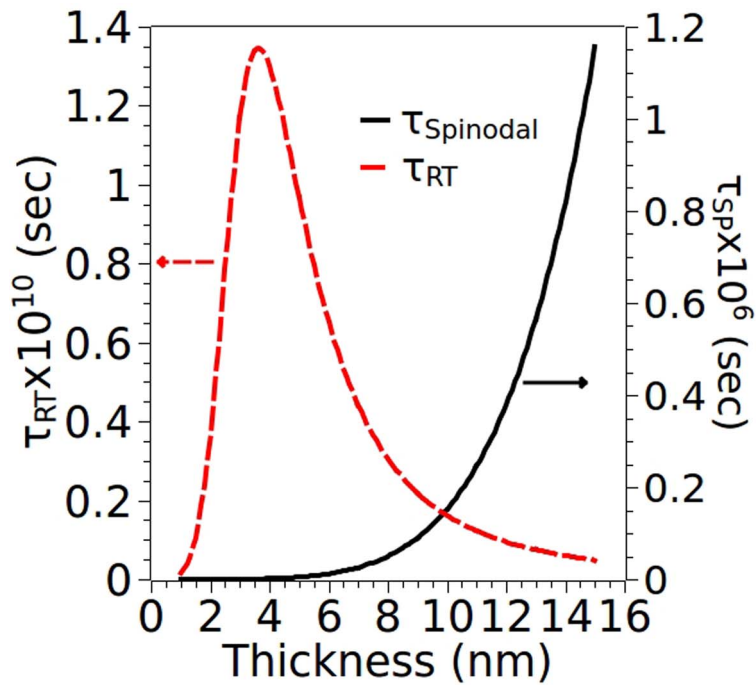
(a)
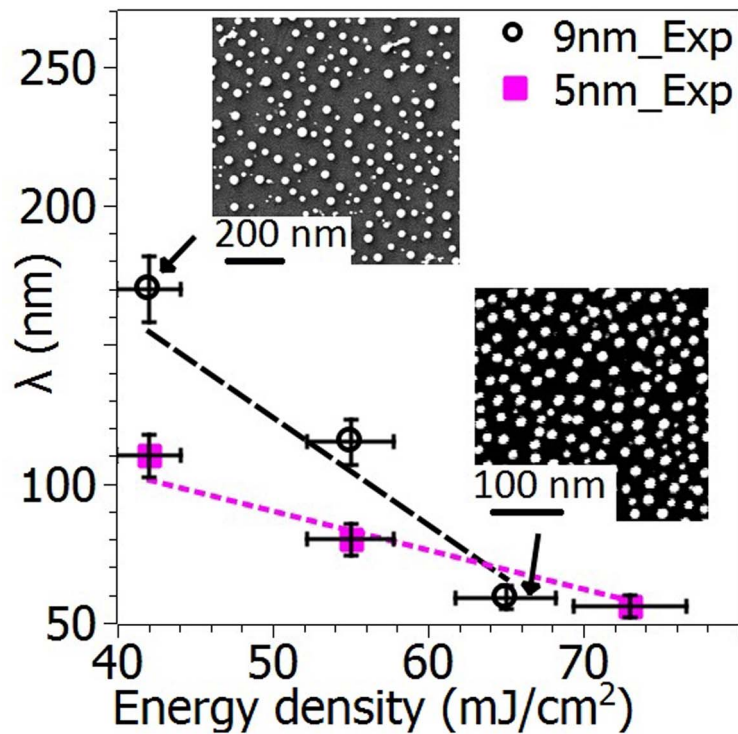
(b)

FIG. 3. (a) Estimate of the RT instability time scale (left y-axis) as a function of film thickness for the experimental conditions used here. The order of magnitude is 10^{-10} s. In contrast, spinodal dewetting in such metal films is a much slower process (right y-axis) with time scales of order 10^{-6} s. (b) Nanoparticle spacing as a function of varying laser energy density for Au films of 9 (dashed line) and 5 nm (dotted line) films. Symbols show experimental measurements while the lines show theoretical predictions. The inset SEM images show the nanoparticle ordering for the 9 nm thick Au film at two different laser energies.

size could be changed for a fixed spacing. However, practical implementation of this pressure-driven instability to potential applications also requires the flexibility in tuning spacing of the nanoparticles. This can be achieved by noting that varying the magnitude of P_Z can change the patterning length scales. From the thermal model result, Fig. 1(b), increasing laser energy density E increases the magnitude of the P_Z force due to the increased T_Z and this in turn should lead to a decrease in length scale through Eq. (8). This result is depicted in Fig. 3(b) for measurements done on Au films of two different thickness. Clearly, increasing the laser energy density leads to substantial decrease in the nanoparticle spacings. In addition, the decreasing length scale predicted by theory calculations (dashed line) is in very good agreement with the experimental measurements (symbols).

VI. CONCLUSION

In this work we show a new way to synthesize nanoparticle arrays on a substrate with *independent* control of size and spacing, which overcomes some limitations of spinodal dewetting length scales. The approach is based on applying the Rayleigh Taylor instability to the nanoscale, a first such demonstration, since this instability, thus far, has only been observed in macroscopic systems. Theoretical arguments show that when thin films are rapidly melted inside a bulk fluid, the ensuing gas pressure gradients can produce huge acceleration forces that can destabilize the film leading to the RT instability and predictable nanoscale sizes. Experimental studies performed for nanosecond pulsed laser melting of Au films in glycerol agreed with the theory. Nanoparticles with a highly monomodal size could be synthesized. Importantly, the spacings between nanoparticles was independent of the film thickness and depended primarily on the pressure gradients, which could be controlled by the laser energy. Since the theory underlying this nanoscale Rayleigh-Taylor instability appears independent of the type of thin film material and/or substrate, this technique could be widely applied to synthesis of nanoparticles from many different materials classes i.e. polymers, ceramics, or metals.

ACKNOWLEDGEMENTS

[1] A. Shipway, E. Katz, and I. Willner, "Nanoparticle arrays on surfaces for electronic, optical, and sensor applications," ChemPhysChem **1**, 18–52 (2000).

[2] I. Robel, V. Subramanian, M. Kuno, and P. Kamat, "Quantum dot solar cells. harvesting light energy with cdse nanocrystals molecularly linked to mesoscopic tio2 films," Journal of the American Chemical Society **128**, 2385–2393 (2006).

[3] S. Maier and H. Atwater, "Plasmonics: Localization and guiding of electromagnetic energy in metal/dielectric structures," Journal of Applied Physics **98** (2005).

[4] Z. Zhong, Y. Yin, B. Gates, and Y. Xia, "Preparation of mesoscale hollow spheres of tio2 and sno2 by templating against crystalline arrays of polystyrene beads," Advanced Materials **12**, 206+ (2000).

[5] J. Hulteen, D. Treichel, M. Smith, M. Duval, T. Jensen, and R. Van Duyne, "Nanosphere lithography: Size-tunable silver nanoparticle and surface cluster arrays," Journal of Physical Chemistry B **103**, 3854–3863 (1999).

[6] J. Jiang, J. P. Liu, X. T. Huang, Y. Y. Li, R. M. Ding, X. X. Ji, Y. Y. Hu, Q. B. Chi, and Z. H. Zhu, "General synthesis of large-scale arrays of one-dimensional nanostructured co3o4 directly on heterogeneous substrates," Crystal Growth & Design **10**, 70–75 (2010).

[7] M. Alavirad, L. Roy, and P. Berini, "Optimization of plasmonic nanodipole antenna arrays for sensing applications," IEEE Journal of Selected Topics in Quantum Electronics **20** (2014).

[8] X. Zou, H. Fan, Y. Tian, and S. Yan, "Synthesis of cu2o/zno hetero-nanorod arrays with enhanced visible light-driven photocatalytic activity," Crystengcomm **16**(6), 1149–1156 (2014).

[9] J. Cui, S. B. Adeloju, and Y. Wu, "Integration of a highly ordered gold nanowires array with glucose oxidase for ultra-sensitive glucose detection," Analytica Chimica Acta **809**, 134–140 (2014).

[10] J. Bischof, D. Scherer, S. Herminghaus, and P. Leiderer, "Dewetting modes of thin metallic films: nucleation of holes and spinodal dewetting," Phys. Rev. Lett. **77**(8), 1536–1539 (1996).

[11] R. Seemann, S. Herminghaus, and K. Jacobs, "Dewetting patterns and molecular forces," Phys. Rev. Lett. **86**, 5534–37 (2001).

[12] J. Trice, D. G. Thomas, C. Favazza, R. Sureshkumar, and R. Kalyanaraman, "Investigation of pulsed laser induced dewetting in nanoscopic Co films: Theory and experiments," Phys. Rev. B **75**, 235439 (2007).

[13] A. Vrij and J. T. G. Overbeek, "Rupture of Thin Liquid Films Due to Spontaneous Fluctuations in Thickness," J. Am. Chem. Soc. **90**, 3074–78 (1968).

[14] G. Reiter, "Dewetting of thin polymer films," Phys. Rev. Lett. **68**(1), 75–78 (1992).

[15] C. Favazza, R. Kalyanaraman, and R. Sureshkumar, "Robust nanopatterning by laser-induced dewetting of metal nanofilms," Nanotechnology **17**, 4229–34 (2006).

[16] J. Trice, C. Favazza, D. Thomas, H. Garcia, R. Kalyanaraman, and R. Sureshkumar, "Novel self-organization mechanism in ultrathin liquid films: theory and experiment," Phys. Rev. lett. **101**(1), 017802 (2008).

[17] C. V. Thompson, "Solid-state dewetting of thin films," Annual Review of Materials Research **42**, 399–434 (2012).

[18] E. Meyer and H. Braun, "Controlled dewetting processes on microstructured surfaces - a new procedure for thin film microstructuring," Macromolecular Materials and Engineering **276**, 44–50 (2000).

[19] K. Kargupta, R. Konnur, and A. Sharma, "Instability and pattern formation in thin liquid films on chemically heterogeneous substrates," Langmuir **16**, 10243–10253 (2000).

[20] R. Konnur, K. Kargupta, and A. Sharma, "Instability and morphology of thin liquid films on chemically heterogeneous substrates," Physical Review Letters **84**, 931–934 (2000).

[21] D. H. Sharp, "An overview of rayleigh-taylor instability," Physica D: Nonlinear Phenomena **12**(1), 3–18 (1984).

[22] G. Taylor, "The instability of liquid surfaces when accelerated in a direction perpendicular to their planes. I," Proceedings of the Royal Society of London. Series A. Mathematical and Physical Sciences **201**(1065), 192–196 (1950).

[23] L. Rayleigh, "Investigation of the character of the equilibrium of an incompressible heavy fluid of variable density," Proceedings of the London Mathematical Society **s1-14**(1), 170–177 (1882).

[24] K. Park, M. Ricotti, T. Di Matteo, and C. S. Reynolds, "Rayleigh-taylor instability of ionization front around black holes," Monthly Notices of the Royal Astronomical Society **437**, 2856–2864 (2014).

[25] S. Woosley and T. Weaver, "The evolution and explosion of massive stars .2. explosive hydrodynamics and nucleosynthesis," Astrophysical Journal Supplement Series **101**, 181–235 (1995).

[26] W. Hillebrandt and J. Niemeyer, "Type ia supernova explosion models," Annual Review of Astronomy and Astrophysics **38**, 191–230 (2000).

[27] E. Ott, "Theory of rayleigh-taylor bubbles in the equatorial ionosphere," Journal of Geophysical Research **83**(A5), 2066–2070 (1978).

[28] P. Sultan, "Linear theory and modeling of the rayleigh-taylor instability leading to the occurrence of equatorial spread f," Journal of Geophysical Research: Space Physics (1978–2012) **101**(A12), 26875–26891 (1996).

[29] H. Chen, B. Hilko, and E. Panarella, "The rayleigh-taylor instability in the spherical pinch," Journal of Fusion Energy **13**(4), 275–280 (1994).

[30] S. Bodner, "Rayleigh-taylor instability and laser-pellet fusion," Physical Review Letters **33**(13), 761–764 (1974).

[31] S. Kawata, T. Kurosaki, K. Noguchi, T. Suzuki, S. Koseki, D. Barada, Y. Y. Ma, A. I. Ogoyski, J. J. Barnard, and B. G. Logan, "Wobblers and rayleigh-taylor instability mitigation in hif target implosion," Nuclear Instruments & Methods in Physics Research Section A-Accelerators Spectrometers Detectors and Associated Equipment **733**, 211–215 (2014); *19th International Symposium on Heavy Ion Inertial Fusion (HIF), Berkeley, CA*, AUG 12–17 (2012).

[32] M. Tabak, J. Hammer, M. Glinsky, W. Kruer, S. Wilks, J. Woodworth, E. Campbell, M. Perry, and R. Mason, "Ignition and high-gain with ultrapowerful lasers," Physics of Plasmas **1**, 1626–1634 (1994); *35th Annual Meeting of the Division-of-Plasma-Physics of the American-Physical-Society, ST LOUIS, MO*, NOV 01–05 (1993).

[33] A. Oron, S. Davis, and S. Bankoff, "Long-scale evolution of thin liquid films," Reviews of Modern Physics **69**, 931–980 (1997).

[34] R. Scardovelli and S. Zaleski, "Direct numerical simulation of free-surface and interfacial flow," Annual Review of Fluid Mechanics **31**, 567–603 (1999).

[35] S. Unverdi and G. Tryggvason, "A front-tracking method for viscous, incompressible, multi-fluid flows," Journal of Computational Physics **100**, 25–37 (1992).

[36] A. Vrij, "Possible mechanism for the spontaneous rupture of thin, free liquid films," Discuss. Faraday Soc. **42**, 23–27 (1966).

[37] A. Sharma and R. Khanna, "Pattern Formation in Unstable Thin Liquid Films," Phys. Rev. Lett. **81**, 3463–66 (1998).

[38] S. Herminghaus, K. Jacobs, K. Mecke, J. Bischof, A. Fery, M. Ibn-Elhaj, and S. Schlagowski, "Spinodal dewetting in liquid crystal and liquid metal films," Science **282**, 916–919 (1998).

[39] M. Bestehorn and D. Merkt, "Regular surface patterns on rayleigh-taylor unstable evaporating films heated from below," Phys. Rev. Lett. **97**, (127802) (2006).

[40] X. Y. Chen, J. Lin, J. M. Liu, and Z. G. Liu, "Formation and evolution of self-organized hexagonal patterns on silicon surface by laser irradiation in water," Applied Physics A-Materials Science & Processing **94**, 649–656 (2009).

[41] H. Park, D. Kim, C. Grigoropoulos, and A. Tam, "Pressure generation and measurement in the rapid vaporization of water on a pulsed-laser-heated surface," Journal of Applied Physics **80**, 4072–4081 (1996).

[42] Y. Dou, L. Zhigilei, N. Winograd, and B. Garrison, "Explosive boiling of water films adjacent to heated surfaces: A microscopic description," Journal of Physical Chemistry A **105**, 2748–2755 (2001).

[43] F. Lang and P. Leiderer, "Liquid-vapour phase transitions at interfaces: sub-nanosecond investigations by monitoring the ejection of thin liquid films," New Journal of Physics **8**, 1–10 (2006).

[44] R. Birkhoff, L. Painter, and J. Heller, Jr., "Optical and dielectric functions of liquid glycerol from gas photoionization measurements," The Journal of Chemical Physics **69**, 4185 (1978).

[45] D. Linde (ed.), *The CRC Handbook of Chemistry and Physics* (CRC Press, Boca Raton, 1992).

[46] M. Khenner, S. Yadavali, and R. Kalyanaraman, "Formation of organized nanostructures from unstable bilayers of thin metallic liquids," Phys. Fluids **23**, 122105 (2011).

[47] J. Prentice, "Coherent, partially coherent and incoherent light absorption in thin-film multilayer structures," Journal of Physics D-Applied Physics **33**, 3139–3145 (2000).

[48] R. Reid, J. Prausnitz, and E. M. Boling, *The Properties of Gases and Liquids*, 5th ed. (McGraw Hill Education, 2001).

[49] S. Yadavali, M. Khenner, and R. Kalyanaraman, "Pulsed laser dewetting of au films: Experiments and modeling of nanoscale behavior," J. Mat. Res. **28**, 1–9 (2013).

[50] See supplementary material at http://dx.doi.org/10.1063/1.4871482 for nanomaterials synthesis by a novel phenomenon: The nanoscale rayleigh-taylor instability.

[51] R. Craster and O. Matar, "Dynamics and stability of thin liquid films," Reviews of Modern Physics **81**(3), 1131 (2009).

[52] A. Sharma and E. Ruckenstein, "Finite-Amplitude Instability of Thin Free and Wetting Films: Prediction of Lifetimes," Langmuir **2**, 480–494 (1986).

[53] H. Bonnemann and R. Richards, "Nanoscopic metal particles - synthetic methods and potential applications," European Journal of Inorganic Chemistry 2455–2480 (2001).